

---

---

# <sup>64</sup>Cu-ATSM Reflects pO<sub>2</sub> Levels in Human Head and Neck Cancer Xenografts but Not in Colorectal Cancer Xenografts: Comparison with <sup>64</sup>CuCl<sub>2</sub>

Fan Li<sup>1</sup>, Jesper T. Jørgensen<sup>1</sup>, Julie Forman<sup>2</sup>, Anders E. Hansen<sup>1,3</sup>, and Andreas Kjaer<sup>1</sup>

<sup>1</sup>Department of Clinical Physiology, Nuclear Medicine & PET and Cluster for Molecular Imaging, Rigshospitalet and University of Copenhagen, Copenhagen, Denmark; <sup>2</sup>Department of Biostatistics, University of Copenhagen, Copenhagen, Denmark; and <sup>3</sup>Center for Nanomedicine and Theranostics, Technical University of Denmark, Kongens Lyngby, Denmark

The hypoxia PET tracer <sup>64</sup>Cu-diacetyl-bis(*N*<sup>4</sup>-methylthiosemicarbazone) (<sup>64</sup>Cu-ATSM) has shown promising results in clinical studies. However, concerns have been raised with regard to the possible effect of copper metabolism and free copper on tumor uptake and thereby the robustness of <sup>64</sup>Cu-ATSM as a hypoxia marker. In this study, accumulation and distribution of <sup>64</sup>Cu-ATSM and <sup>64</sup>CuCl<sub>2</sub> in tumor tissue were compared with partial pressure of oxygen (pO<sub>2</sub>) probe measurements. **Methods:** One-hour dynamic PET scans were performed on nude mice bearing subcutaneous human head and neck tumors (FaDu) and human colorectal tumors (HT29) after administration of either <sup>64</sup>Cu-ATSM or <sup>64</sup>CuCl<sub>2</sub>. Subsequently, tracks were generated and track markers were positioned in tumors to allow for registration of their exact location on the high-resolution CT scan. After completion of the CT scan, pO<sub>2</sub> probe measurements were performed along each track. PET and CT images were coregistered and ROIs drawn on the basis of the location of track markers and pO<sub>2</sub> probe measurement depth. A linear mixed model for repeated measures was applied for the comparison of PET tracer uptake to corresponding pO<sub>2</sub> values. **Results:** Comparable uptake of <sup>64</sup>Cu-ATSM and <sup>64</sup>CuCl<sub>2</sub> was found in the kidney, muscle, and liver of all animals, but <sup>64</sup>CuCl<sub>2</sub> showed a higher uptake 10–60 min after injection in both tumor models. Significant differences were also found for both tumor-to-muscle and tumor-to-liver ratios. The intratumoral distribution of <sup>64</sup>Cu-ATSM, but not <sup>64</sup>CuCl<sub>2</sub>, showed a significant negative relationship with pO<sub>2</sub> measurements in FaDu tumors. However, this relationship was not found in HT29 tumors. **Conclusion:** <sup>64</sup>Cu-ATSM and <sup>64</sup>CuCl<sub>2</sub> displayed different uptake in tumors. In human head and neck xenografts, <sup>64</sup>Cu-ATSM but not <sup>64</sup>CuCl<sub>2</sub> reflected pO<sub>2</sub> measurements, indicating that <sup>64</sup>Cu-ATSM is a hypoxia-specific marker in this tumor type. However, data from colorectal cancer xenografts indicated that <sup>64</sup>Cu-ATSM may not be a hypoxia marker in all tumor types.

**Key Words:** PET/CT; <sup>64</sup>Cu-ATSM; hypoxia; pO<sub>2</sub> probe; head and neck cancer xenograft

**J Nucl Med 2016; 57:437–443**

DOI: 10.2967/jnumed.115.155663

**T**umor hypoxia is associated with an aggressive tumor phenotype and radio- and chemotherapy resistance (1–4). A variety of techniques have been applied to assess hypoxia, but partial pressure of oxygen (pO<sub>2</sub>) probe measurements are currently regarded as the gold standard and have been extensively used to study the relationship between tumor oxygenation and clinical outcome (1,5–7). However, this method has several limitations due to the inaccessibility of some tumors for needle placement, the limited sampling volume, and the invasive nature of the procedure (8). In addition, the oxygen electrode is unable to distinguish between necrotic and viable hypoxic areas, and insertion of the probe disrupts the tissue at the site of measurement.

Tissue oxygenation can also be quantified with noninvasive imaging techniques, such as MRI, electron paramagnetic resonance, and PET (9,10), and <sup>64</sup>Cu-diacetyl-bis(*N*<sup>4</sup>-methylthiosemicarbazone) (<sup>64</sup>Cu-ATSM) is one of several PET tracers currently under evaluation for imaging of tumor hypoxia. <sup>64</sup>Cu-ATSM has a high tumor-to-background ratio and has shown promising results in small clinical studies, in which the tumor-to-muscle ratio was able to predict treatment outcome (11–13). However, the robustness of <sup>64</sup>Cu-ATSM as a marker of hypoxia has been questioned, because preclinical studies have reported temporal changes in tumor uptake and cell-type-specific differences in hypoxia selectivity (14–26). Table 1 provides an overview of major studies using <sup>64</sup>Cu-ATSM in small-animal tumor xenograft models.

The mechanism responsible for <sup>64</sup>Cu-ATSM retention is not completely understood, but *in vitro* studies have indicated that the <sup>64</sup>Cu-ATSM complex undergoes reduction by free diffusion after entering the cells (27–29). In normoxic cells, <sup>64</sup>Cu-ATSM is rapidly reoxidized and consequently able to leave the cell again by free diffusion. In hypoxic cells, reoxidation occurs at a slower rate, leaving enough time for dissociation of the unstable [<sup>64</sup>Cu-ATSM]<sup>−</sup>. The radioactive copper isotope then becomes part of the intracellular copper pool, and some studies have indicated that there also appears to be an efflux of either radiolabeled <sup>64</sup>Cu-ATSM or copper from cancer cells (30–32). Moreover, studies of copper metabolism using <sup>64</sup>CuCl<sub>2</sub> PET in tumor xenograft mouse models have reported high tumor accumulation in some tissue types (33,34). This is interesting with regard to the proposed trapping mechanism and *in vivo* stability of <sup>64</sup>Cu-ATSM, as copper could both accumulate in tumor tissue and redistribute after dissociation from the <sup>64</sup>Cu-ATSM complex. Indeed, a recent study comparing <sup>64</sup>Cu-ATSM and <sup>64</sup>Cu-acetate

---

Received Feb. 17, 2015; revision accepted Oct. 22, 2015.

For correspondence or reprints contact: Andreas Kjaer, Department of Clinical Physiology, Nuclear Medicine, and PET, Rigshospitalet, Blegdamsvej 9, 2100 Copenhagen, Denmark.

E-mail: akjaer@sund.ku.dk

Published online Nov. 19, 2015.

COPYRIGHT © 2016 by the Society of Nuclear Medicine and Molecular Imaging, Inc.

**TABLE 1**  
Major Studies Using Cu-ATSM in Small-Animal Tumor Models

Ref	Tumor type (origin)	Cell line	Host	Method	Major findings
18	Mu. gliosarcoma	9L	F Fischer 344 rats	PET/ manipulating tumor pO <sub>2</sub>	ATSM uptake could be manipulated by changes in inhaled oxygen content and by hydralazine injection; changes in tumor oxygenation were confirmed by polarographic oxygen needle
21	Mu. prostate AC Hu. H&N SCC	Dunning R3327- AT FaDu	M Fisher- Copenhagen rats Nude rats	PET/IHC	Intratumoral distribution of ATSM in R3327-AT evolved; only late uptake (16–30 h) corresponded well with FMISO accumulation, pO <sub>2</sub> probe measurements, and pimonidazole and Hoechst-33342 staining; ATSM uptake in FaDu did not differ between early (1–2 h) and late scans and had distribution similar to FMISO
25	Mu. mammary AC Mu. fibrosarcoma Mu. gliosarcoma	R3230AC FSA 9L	Fischer 344 rats	PET/ARG/IHC	Close correlation was found between EF5 staining and ATSM accumulation (1 h) in R3230-AC and 9L but not in FSA, which had highest overall uptake; lack of correlation between ATSM distribution and hypoxia in FSA tumors was confirmed by pimonidazole and CAIX staining
23	Mu. melanoma Mu. LLC Mu. colon C Mu. fibrosarcoma	B16 LLC1 Colon26 Meth-A	M C57BL/6 mice M BALB/c mice	ARG/IHC	Different spatial distribution between ATSM and FDG was found in all 4 models; ATSM accumulated primarily in tumor regions with low microvessel density
19	Mu. H&N SCC	SCCVII	F C3H mice	PET/ manipulating tumor pO <sub>2</sub>	No significant difference in ATSM tumor uptake was found between animals breathing carbogen and air; changes in tumor oxygenation were confirmed by pimonidazole staining
15	Mu. gliosarcoma	9L	F Fischer 344 rats	ARG/PET	Strong correlation was found between both early (10 min) and late (24 h) uptake of ATSM and FMISO (2 h)
22	Mu. LLC	LLC1	M C57BL/6 mice	ARG/IHC	Grade of accumulation and spatial distribution differed between ATSM and FDG; discrepancy existed between intratumoral distribution of ATSM and pimonidazole (1 h)
17	Mu. mammary AC	CaNT*	F CBA mice	PET/ manipulating tumor pO <sub>2</sub>	Anesthetics and O <sub>2</sub> level in inhalation mixture can affect ATSM uptake in tumor and normal tissue; tumor oxygenation was confirmed by pO <sub>2</sub> probe measurements and EF5 staining
20	Hu. H&N SCC	FaDu	Nude rats	PET/ARG/IHC	There was continuous increase in tumor uptake during 90-min dynamic scans and further increase at 18 h; spatial distribution of early (1 h) but not late (18 h) ATSM uptake correlated with Hoechst-33342 staining; pimonidazole staining correlated with neither time point
24	Mu. mammary C Hu. prostate AC Hu. H&N SCC	EMT6 PC3 FaDu	BALB/c nude mice	PET/ARG/IHC	Both early (2 h) and late (24 h) ATSM spatial distribution was similar to FAZA (2 h) in FaDu; in PC3 and EMT6 only partial overlap was observed with late uptake of ATSM
16	Mu. mammary AC Mu. mammary C	CaNT* EMT6	F CBA mice F BALB/c mice	PET/ manipulating tumor pO <sub>2</sub> /ARG/IHC	Similarity in biodistribution and T/M of ATSM and acetate and T/M of both tracers was reduced by change in O <sub>2</sub> content of inhalation mixture; EF5 staining correlated with late (16 h) but not early (15 min and 2 h) intratumoral distribution of ATSM and acetate
14	Hu. H&N SCC Hu. colorectal AC Hu. colorectal AC	SQ20b HT29 HCT116	F athymic nude mice	PET/ARG/IHC	ATSM pattern of intratumoral distribution differed from fluorinated nitroimidazoles FMISO, FAZA, and HX4 (80–90 min); ATSM accumulation correlated with Hoechst-33342 but not CAIX or pimonidazole staining in all 3 models

\*Tumor line that cannot be grown ex vivo.

Ref = reference number; Mu. = murine; Hu. = human; AC = adenocarcinoma; SCC = squamous cell carcinoma; LLC = Lewis lung carcinoma; C = carcinoma; H&N = head and neck; F = female; M = male; IHC = immunohistochemistry staining; ARG = autoradiography; ATSM = Cu-ATSM; FMISO = <sup>18</sup>F-fluoromisonidazole; CAIX = carbonic anhydrase IX; FDG = <sup>18</sup>F-FDG; FAZA = <sup>18</sup>F-fluoroazomycin; HX4 = <sup>18</sup>F-2-nitroimidazole nucleoside analog; T/M = tumor-to-muscle ratio.

uptake in tumor-bearing mice found great similarity between the two tracers (16). In addition, *in vivo* stability experiments indicated that a fraction of  $^{64}\text{Cu}$  found in blood was not associated with the  $^{64}\text{Cu}$ -ATSM complex within a few minutes after tracer administration (16).

Oxygen probe measurements have previously been applied to compare the uptake of PET tracers to average tumor  $\text{pO}_2$  values (35–37). Moreover, the technique has also been used for evaluation of the spatial distribution of hypoxia PET tracers in a few studies (21,38,39). In this study, uptake of  $^{64}\text{Cu}$ -ATSM and  $^{64}\text{CuCl}_2$  was measured in human tumor xenograft-bearing nude mice using small-animal PET, and the intratumoral distribution was compared with  $\text{pO}_2$  probe measurements.

## MATERIALS AND METHODS

### Tumor Model

All experiments were performed under national and European Union–approved guidelines for animal welfare. Human head and neck cancer (FaDu) and colorectal cancer (HT29) cell lines (ATCC) were cultured at  $37^\circ\text{C}$  and 5%  $\text{CO}_2$  in minimum essential medium and McCoy 5A medium, respectively, both supplemented with 10% fetal calf serum and 1% penicillin–streptomycin (all from Invitrogen Co.). Seven-week-old female nude NMRI mice (Taconic Europe) had  $10^7$  cells, dissolved in 100  $\mu\text{L}$  of medium mixed with 100  $\mu\text{L}$  of Matrigel Basement Membrane Matrix (BD-Biosciences), subcutaneously inoculated into each flank. Throughout the experiment, the mice were regularly weighed and tumor dimensions measured using a caliper.

### Experimental Setup

$^{64}\text{CuCl}_2$  and  $^{64}\text{Cu}$ -ATSM were produced and synthesized by Risø National Laboratory, Technical University of Denmark. Before the procedure, the animals were weighed and randomized into 4 groups of 4 animals each. All tumors used in this study had diameters of about 10 mm in each dimension. During all procedures, the mice were anesthetized using a mixture of 3% sevoflurane (Abbott Scandinavia AB) mixed with 35%  $\text{O}_2$  in  $\text{N}_2$ .  $^{64}\text{Cu}$ -ATSM or  $^{64}\text{CuCl}_2$  was injected into a tail vein, and the exact dose calculated ( $^{64}\text{Cu}$ -ATSM:  $8.96 \pm 0.65$  MBq (mean  $\pm$  SD);  $^{64}\text{CuCl}_2$ :  $9.47 \pm 1.55$  MBq) on the basis of measurements of the syringe before and after injection using a radioisotope calibrator (HRC-120; Amersham). Immediately after the injection, the mice were placed on a scanner bed, and the subcutaneous tumors on each flank were positioned for optimal needle access and fixed to eliminate movement. One-hour dynamic scans were performed on a microPET Focus 120 (Siemens Medical Solutions) with a resolution of 1.18 mm (sagittal), 1.13 mm (coronal), and 1.44 mm (transversal) at the center of the field of view. The resulting list-mode data were postprocessed using 3-dimensional maximum a priori algorithms into  $256 \times 256 \times 95$  image matrices with a voxel size of 0.43  $\text{mm}^3$ . For each mouse, frames were defined so they contained data from 10 to 20, 20 to 30, 30 to 40, 40 to 50, and 50 to 60 min from injection to the start of PET acquisition.

After the PET acquisition, two to three 24-gauge vein catheters (Becton Dickinson A/S) were pierced through each tumor and the catheter needle retracted. The plastic catheter tubes were left in the tumor tissue as track markers and for later guidance of  $\text{pO}_2$  probe insertion. There was a minimum of 3–4 mm between the individual tracks. The animal bed was moved to a small-animal CT scanner and a 7-min CT scan performed. Immediately after completion of the CT scan, the animals were moved to a preheated  $\text{pO}_2$  measurement platform and a fiber-optic oxygen-sensitive probe (OxyLite 4000; Oxford Optronix) was used to measure local oxygen tension in tumors. More detail on oxygen probe measurement is provided in the supplemental data (available at <http://jnm.snmjournals.org>).

### Data and Statistical Analysis

For each group,  $\text{pO}_2$  measurements were pooled and cumulative frequency plots of  $\text{pO}_2$  measurements were used to compare the distribution. Values below 1.5 mm Hg, equal to 2 times the measurement accuracy of the OxyLite measurement system, were excluded from the analysis. After this step, there were 108, 98, 102, and 127 data points left for further analysis in the FaDu  $^{64}\text{Cu}$ -ATSM, FaDu  $^{64}\text{CuCl}_2$ , HT29  $^{64}\text{Cu}$ -ATSM, and HT29  $^{64}\text{CuCl}_2$  groups, respectively.

All image data were analyzed using Inveon software (Siemens Medical Solutions). PET and CT images were coregistered in 3 dimensions by an affine registration algorithm and visually inspected. Regions of interest (ROIs) were drawn on tumor, muscle, liver, and kidney tissue and uptake calculated as mean %ID/g (percentage injected dose per gram of tissue), tumor-to-muscle ratio, and tumor-to-liver ratio for comparison of image-derived biodistribution. In addition, multiple 20-voxel spheric ROIs ( $\sim 0.6$   $\text{mm}^3$ ) were placed along each catheter track. This first ROI was placed immediately under the skin, and the distance between each data point was the same as for the  $\text{pO}_2$  measurements ( $\sim 0.5$  mm). The uptakes of all regions along each track were calculated as mean %ID/g.

A linear mixed model adjusting for serial correlation (autoregressive) of repeated measurements was used to assess the association between uptake of  $^{64}\text{Cu}$ -ATSM or  $^{64}\text{CuCl}_2$  and the corresponding  $\text{pO}_2$  probe measurements when both tumor model and time effect was considered. It was assumed that variation caused by tracer type, tumor model, time, and  $\text{pO}_2$  and the interactions between them was fixed and that the effect of individual animals was random. Statistical analysis was performed with SPSS statistical software, version 20.0 (IBM Corp.), and Prism 5 (GraphPad Software, Inc.) was used for illustrations. The cumulative frequency plots were visualized using in-house–constructed algorithm using Matlab (version 2014b; The MathWorks, Inc.). PET data are presented as mean  $\pm$  SEM. A *P* value of less than 0.05 was considered statistically significant in all analyses.

## RESULTS

### Comparison of $^{64}\text{Cu}$ -ATSM and $^{64}\text{CuCl}_2$ Uptake

The image-derived biodistribution of  $^{64}\text{Cu}$ -ATSM and  $^{64}\text{CuCl}_2$  in different tissues from 10 to 60 min after injection was investigated (Fig. 1). Uptake of  $^{64}\text{Cu}$ -ATSM was comparable to that of  $\text{CuCl}_2$  in muscle, kidney, and liver tissue in both tumor models. However, a higher accumulation of  $^{64}\text{CuCl}_2$  than of  $^{64}\text{Cu}$ -ATSM was found in both FaDu and HT29 tumors, resulting in significantly higher tumor-to-muscle and tumor-to-liver ratios (Figs. 2 and 3). Also, a higher variation in tumor and liver uptake between animals was observed in the  $^{64}\text{CuCl}_2$  group.

### Intratumoral $\text{pO}_2$ Measurements

The  $\text{pO}_2$  values obtained with the oxygen probe in FaDu tumors ranged from  $-0.55$  to 53 mm Hg in the  $^{64}\text{Cu}$ -ATSM group and  $-0.72$  to 46 mm Hg in the  $^{64}\text{CuCl}_2$  group. In HT29 tumors, the  $\text{pO}_2$  values ranged from  $-0.60$  to 57.74 mm Hg in the  $^{64}\text{Cu}$ -ATSM group and  $-0.86$  to 60.04 mm Hg in the  $^{64}\text{CuCl}_2$  group. To evaluate the compatibility of  $\text{pO}_2$  measurement in the  $^{64}\text{Cu}$ -ATSM and  $^{64}\text{CuCl}_2$  groups, the relative frequency of readings  $\leq 2.5$ ,  $\leq 5$ , and  $\leq 10$  mm Hg and the mean and median  $\text{pO}_2$  were determined on the basis of the cumulative median frequency plots (Supplemental Figs. 2 and 3). In the FaDu tumor-bearing mice, the  $^{64}\text{Cu}$ -ATSM group had 64%, 68%, and 77% of measurements  $\leq 2.5$  mm Hg,  $\leq 5$  mm Hg, and  $\leq 10$  mm Hg, respectively. The respective percentages in the  $^{64}\text{CuCl}_2$  group were 60%, 64%, and 72%. In the HT29 tumor-bearing mice, the  $^{64}\text{Cu}$ -ATSM group had 74%, 78%, and 81% of measurements  $\leq 2.5$  mm Hg.

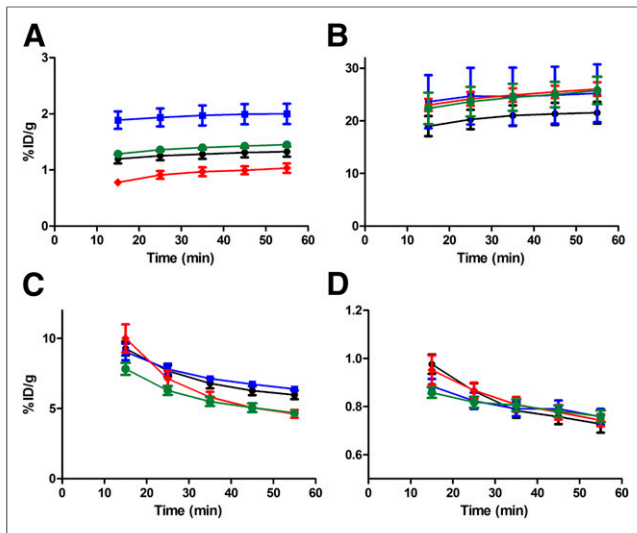


**FIGURE 1.** Image-derived biodistribution of  $^{64}\text{Cu}$ -ATSM and  $^{64}\text{CuCl}_2$  obtained from dynamic PET scans performed 10–60 min after injection. Uptake in FaDu tumor-bearing mice of  $^{64}\text{Cu}$ -ATSM (black symbols) ( $n = 4$ ) and  $^{64}\text{CuCl}_2$  (blue symbols) ( $n = 4$ ) and uptake in HT29 mice of  $^{64}\text{Cu}$ -ATSM (red symbols) ( $n = 4$ ) and  $^{64}\text{CuCl}_2$  (green symbols) ( $n = 4$ ) is given as mean %ID/g  $\pm$  SEM in tumor (A), liver (B), kidney (C), and muscle (D). Animals were anesthetized during scans by breathing 3% sevoflurane mixed with 35%  $\text{O}_2$  in  $\text{N}_2$ .

Hg,  $\leq 5$  mm Hg, and  $\leq 10$  mm Hg, respectively. The respective percentages in the  $^{64}\text{CuCl}_2$  group were 66%, 76%, and 81%.

#### Intratumoral $^{64}\text{CuCl}_2$ and $^{64}\text{Cu}$ -ATSM Uptake and $\text{pO}_2$ Measurements

The possible association between the  $\text{pO}_2$  probe measurements and  $^{64}\text{Cu}$ -ATSM and  $^{64}\text{CuCl}_2$  uptake in corresponding regions in FaDu and HT29 tumors was evaluated by a linear mixed model (Table 2). We found a significant negative association between  $\text{pO}_2$  and the mean %ID/g of  $^{64}\text{Cu}$ -ATSM in FaDu tumors ( $P < 0.0001$ ), whereas no significant association was found between  $\text{pO}_2$  and  $^{64}\text{CuCl}_2$  ( $P = 0.248$ ). In the HT29 tumors, no significant association was found between either  $^{64}\text{Cu}$ -ATSM or  $^{64}\text{CuCl}_2$  uptake and  $\text{pO}_2$  ( $P = 0.590$  and  $P = 0.132$ , respectively) (Table 2). In FaDu tumors, the association between  $\text{pO}_2$  and mean  $^{64}\text{Cu}$ -ATSM was found to be significant at all time points. The changes in regression coefficients over time were small and nonsystematic (Table 3). Figures 4 and 5 show the relationships between tracer uptake and  $\text{pO}_2$  at 50–60 min after injection in FaDu and HT29 tumors, respectively.

#### DISCUSSION

The mechanism responsible for  $^{64}\text{Cu}$ -ATSM retention is not fully understood, and recently there has been a focus on the possible effect of copper metabolism on tumor uptake (16,33). A recent study compared  $^{64}\text{Cu}$ -ATSM and  $^{64}\text{Cu}$ -acetate uptake in tumor-bearing mice and reported that the two tracers had similar biodistributions (16). Moreover, the immunohistochemical hypoxia marker 2-(2-nitro-1*H*-imidazol-1-yl)-*N*-(2,2,3,3,3-pentafluoropropyl)-acetamide (EF5) correlated with the late (16 h), but not the early (15 min and 2 h), intratumoral tracer distribution of both  $^{64}\text{Cu}$ -ATSM and  $^{64}\text{Cu}$ -acetate (16). It was previously reported that the relationship between  $^{64}\text{Cu}$ -ATSM and EF5 accumulation in tumors is dependent on tissue type (25). However, the similarity

in biodistribution and tumor uptake shown by  $^{64}\text{Cu}$ -acetate and  $^{64}\text{Cu}$ -ATSM could indicate that a large fraction of the  $^{64}\text{Cu}$  that had initially bound to ATSM dissociated.

In this study, we also found a similar accumulation of copper in kidney, liver, and muscle tissue using  $^{64}\text{Cu}$ -ATSM and  $^{64}\text{CuCl}_2$  PET. However, in contrast,  $^{64}\text{CuCl}_2$  showed a higher uptake than  $^{64}\text{Cu}$ -ATSM in both HT29 and FaDu tumors at all time points. Also, different relationships between  $\text{pO}_2$  and the spatial distribution of  $^{64}\text{CuCl}_2$  and  $^{64}\text{Cu}$ -ATSM were found. The level of tumor uptake and tumor-to-background ratios of both  $^{64}\text{Cu}$ -ATSM and  $^{64}\text{CuCl}_2$  found in this study seems to be lower than has previously been reported (14,20,33). However, during the 1-h dynamic scans, the tumor-to-muscle ratios of both  $^{64}\text{Cu}$ -ATSM and  $^{64}\text{CuCl}_2$  continued to increase and did not reach a plateau. Importantly, the different imaging time points and anesthetic procedures applied in the different studies complicate a direct comparison of results. It has previously been shown that both anesthetics and level of oxygen in anesthetic gas mixtures can influence tissue uptake of both  $^{64}\text{Cu}$ -ATSM and copper (16,17). Therefore, to avoid fluctuations in uptake, the level of the anesthetic gas mixture was strictly kept at a constant level during all procedures from tracer injection until completion of  $\text{pO}_2$  probe measurements. However, the experimental setup has likely contributed to slower accumulation and clearance from the background than would be seen when the tracer is allowed to distribute in an unanesthetized animal (16,17).

A previous study on nude rats with FaDu tumors found no correlation between hypoxia marker, pimonidazole, and intratumoral spatial distribution of  $^{64}\text{Cu}$ -ATSM 1 and 18 h after injection (20). In contrast, another study using the same tumor model found that there was no temporal change in the intratumoral distribution of  $^{64}\text{Cu}$ -ATSM early (2 h) or late (16 h) after injection and that  $\text{pO}_2$  probe measurements from different tumor sections corroborated well with PET images (21). This is consistent with our finding of a negative relationship between  $\text{pO}_2$  probe measurements and the intratumoral spatial distribution of  $^{64}\text{Cu}$ -ATSM in FaDu. However, when we performed the same experiment on mice bearing HT29 tumors no relationship was found. A tumor type-dependent difference between intratumoral  $^{64}\text{Cu}$ -ATSM accumulation and other hypoxic markers has previously been reported by

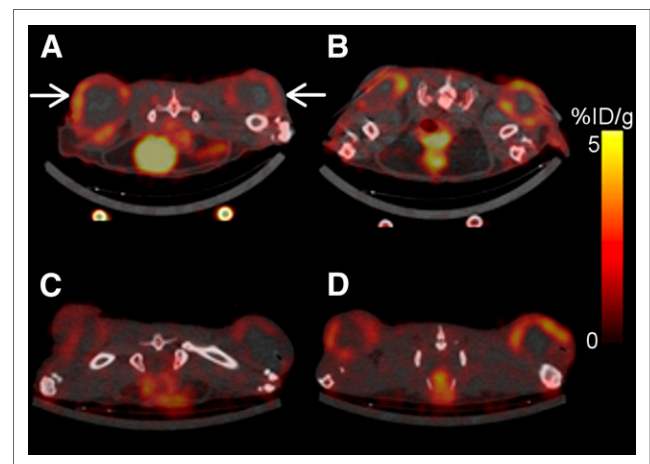


**FIGURE 2.** Representative transaxial PET images 50–60 min after injection of FaDu tumor-bearing mice with  $^{64}\text{Cu}$ -ATSM (A) and  $^{64}\text{CuCl}_2$  (B) and of HT29 tumor-bearing mice with  $^{64}\text{Cu}$ -ATSM (C) and  $^{64}\text{CuCl}_2$  (D) (arrows indicate tumors).

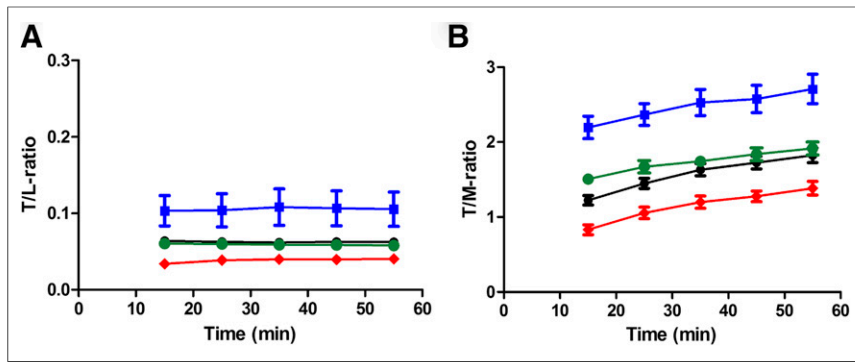


**FIGURE 3.** Tumor-to-liver (A) and tumor-to-muscle (B) ratios from dynamic  $^{64}\text{Cu}$ -ATSM or  $^{64}\text{CuCl}_2$  PET scans performed 10–60 min after injection. Uptake in FaDu mice of  $^{64}\text{Cu}$ -ATSM (black symbols) ( $n = 4$ ) and  $^{64}\text{CuCl}_2$  (blue symbols) ( $n = 4$ ) and uptake in HT29 mice of  $^{64}\text{Cu}$ -ATSM (red symbols) ( $n = 4$ ) and  $^{64}\text{CuCl}_2$  (green symbols) ( $n = 4$ ) is shown. Animals were anesthetized during scans by breathing 3% sevoflurane mixed with 35%  $\text{O}_2$  in  $\text{N}_2$ .

**TABLE 2**

Regression Coefficients for Effect of  $\text{pO}_2$  on PET Tracer Uptake

Group	Estimate	95% confidence interval		P
		Lower	Upper	
FaDu $^{64}\text{Cu}$ -ATSM	-0.0222	-0.0330	-0.0114	<0.0001
FaDu $^{64}\text{CuCl}_2$	0.0066	-0.0046	0.0178	0.2478
HT29 $^{64}\text{Cu}$ -ATSM	-0.0022	-0.0102	0.0058	0.5898
HT29 $^{64}\text{CuCl}_2$	0.0073	-0.0022	0.0169	0.1323

others, and a study comparing the spatial distribution of  $^{64}\text{Cu}$ -ATSM to pimonidazole in mice bearing HT29 tumors also found no relationship (14,25).

$\text{pO}_2$  probe measurements are considered the gold standard for determining tissue oxygenation and are therefore an attractive method for evaluating the performance of hypoxia PET tracers. As previously mentioned, however, this approach has some limitations. We used cumulative median frequency plotting to verify a good similarity between the distributions of  $\text{pO}_2$  readings in the two tumor models before making the comparison with  $^{64}\text{Cu}$ -ATSM and  $^{64}\text{CuCl}_2$  accumulation. However, one limitation to

the oxygen probe is that it cannot distinguish between necrotic and severely hypoxic tissue. Recordings performed on necrotic tumor areas are problematic for the comparison with tracer uptake because these regions consist of nonviable cells unable to accumulate  $^{64}\text{Cu}$ -ATSM, which could be interpreted as hypoxic. FaDu and HT29 tumors grown subcutaneously in nude mice are likely to develop central necrosis, and a significant number of the obtained  $\text{pO}_2$  values were near zero. Therefore, to include only viable tumor tissue,  $\text{pO}_2$  values below 2 times the measurement accuracy of the probe (<1.5 mm Hg) were excluded from the analysis. Also, as probe insertion is invasive, there is a possibility that it induces changes in oxygenation. Using our setup, there is a

risk of inducing changes in microregional tumor oxygenation between the PET scan and the  $\text{pO}_2$  probe recordings, leading to a mismatch between corresponding measurements. Microregional changes in tumor perfusion (acute hypoxia) could also have the same effect. Moreover, the analysis is sensitive with regard to misalignment between ROIs in PET images and the corresponding  $\text{pO}_2$  measurements. Even though the tumors were fixed during needle penetration, movement could affect the coregistration, but any effect is likely limited as the ROIs placed on the PET images covered a much larger subvolume of the tumor than the microregional sample volume of the oxygen probe. However, this discrepancy in volume can also induce variation, as uptake from ROIs represents average values of tracer accumulation within larger regions, potentially comprising microregional differences in oxygenation.

Overall, despite conflicting preclinical findings,  $^{64}\text{Cu}$ -ATSM is a promising PET tracer because it has shown the ability to predict treatment outcome in small patient studies. However, improved understanding of the tissue-specific selectivity and temporal evolution of distribution, also with regard to in vivo stability, is important for optimal application of the tracer. Moreover, it is not clear whether the preclinical findings can be translated into patients. Therefore, further clinical studies are required on whether tumor uptake of  $^{64}\text{Cu}$ -ATSM can be used as a hypoxia marker or, alternatively, to provide other prognostic information.

**TABLE 3**

Estimated Effect of  $\text{pO}_2$  on PET Tracer Uptake at Different Time Points

Minutes	FaDu				HT29			
	$^{64}\text{Cu}$ -ATSM		$^{64}\text{CuCl}_2$		$^{64}\text{Cu}$ -ATSM		$^{64}\text{CuCl}_2$	
	Estimate	P	Estimate	P	Estimate	P	Estimate	P
10–20	-0.0191 (-0.0305; -0.0079)	0.0009	0.0132 (0.0015; 0.0250)	0.0273	-0.0035 (-0.0121; 0.0051)	0.4209	0.0085 (-0.0016; 0.0185)	0.0996
20–30	-0.0211 (-0.0324; -0.0098)	0.0003	0.0083 (-0.0034; 0.0201)	0.1650	-0.0030 (-0.0114; 0.0053)	0.4800	0.0065 (-0.0035; 0.0165)	0.2032
30–40	-0.0194 (-0.0308; -0.0081)	0.0008	0.0068 (-0.0050; 0.0185)	0.2591	-0.0006 (-0.0090; 0.0077)	0.8836	0.0092 (-0.0008; 0.0193)	0.0708
40–50	-0.0201 (-0.0314; -0.0088)	0.0005	0.0091 (-0.0026; 0.0209)	0.1281	-0.0005 (-0.0089; 0.0078)	0.9012	0.0075 (-0.0025; 0.0175)	0.1417
50–60	-0.0291 (-0.0405; -0.0179)	<0.00001	-0.0031 (-0.0149; 0.0086)	0.6019	-0.0030 (-0.0113; 0.0054)	0.4852	0.0054 (-0.0047; 0.0154)	0.2932

Data in parentheses are 95% confidence intervals.

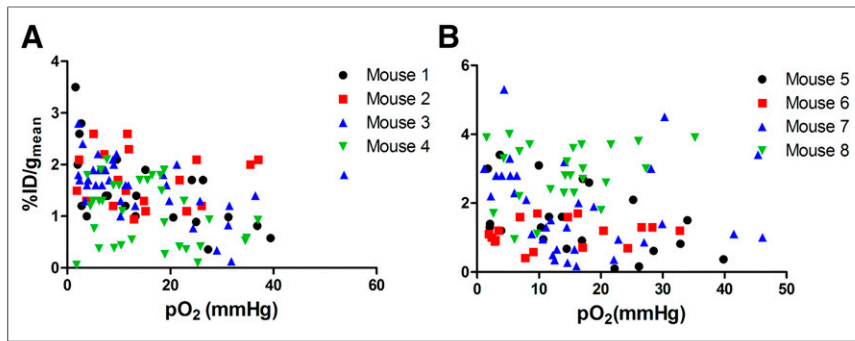


**FIGURE 4.** Comparison between  $pO_2$  probe measurements and tracer uptake (mean %ID/g) in FaDu tumor subvolumes. (A)  $^{64}Cu$ -ATSM 50–60 min after injection. (B)  $^{64}CuCl_2$  50–60 min after injection. Number of tumor subvolumes used for analysis was 108 for  $^{64}Cu$ -ATSM and 96 for  $^{64}CuCl_2$ .

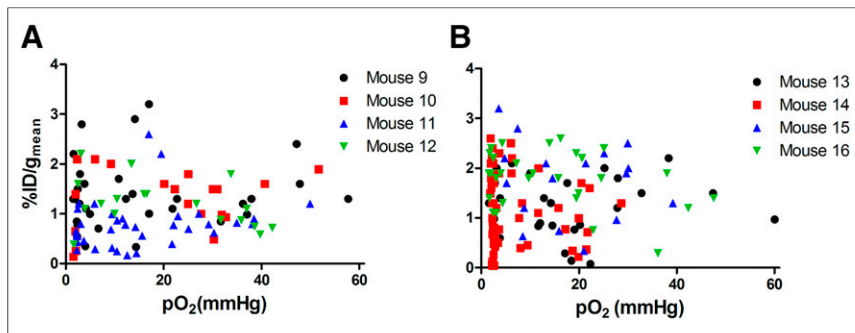


**FIGURE 5.** Comparison between  $pO_2$  measurements and tracer uptake (mean %ID/g) in HT29 tumor subvolumes. (A)  $^{64}Cu$ -ATSM 50–60 min after injection. (B)  $^{64}CuCl_2$  50–60 min after injection. Number of tumor subvolumes used for analysis was 102 for  $^{64}Cu$ -ATSM and 127 for  $^{64}CuCl_2$ .

## CONCLUSION

In human head and neck xenografts,  $^{64}Cu$ -ATSM but not  $^{64}CuCl_2$  reflected  $pO_2$  measurements, indicating that  $^{64}Cu$ -ATSM is indeed a hypoxia marker in this tumor type. However, data from colorectal cancer xenografts indicated that  $^{64}Cu$ -ATSM may not be a hypoxia marker in all tumor types.

## DISCLOSURE

The costs of publication of this article were defrayed in part by the payment of page charges. Therefore, and solely to indicate this fact, this article is hereby marked “advertisement” in accordance with 18 USC section 1734. This work was financially supported by the Lundbeck Foundation, the Novo Nordisk Foundation, the Svend Andersen Foundation, the Arvid Nilsson Foundation, Innovationsfonden, the Research Fund of Rigshospitalet, the Capital Region of Denmark, and the John and Birthe Meyer Foundation. No other potential conflict of interest relevant to this article was reported.

## REFERENCES

1. Brizel DM, Sibley GS, Prosnitz LR, Scher RL, Dewhirst MW. Tumor hypoxia adversely affects the prognosis of carcinoma of the head and neck. *Int J Radiat Oncol Biol Phys.* 1997;38:285–289.
2. Brown JM. The hypoxic cell: a target for selective cancer therapy—eighteenth Bruce F. Cain Memorial Award lecture. *Cancer Res.* 1999;59:5863–5870.

3. Hockel M, Schlenger K, Aral B, Mitze M, Schaffer U, Vaupel P. Association between tumor hypoxia and malignant progression in advanced cancer of the uterine cervix. *Cancer Res.* 1996;56:4509–4515.
4. Nordmark M, Bentzen SM, Rudat V, et al. Prognostic value of tumor oxygenation in 397 head and neck tumors after primary radiation therapy: an international multi-center study. *Radiother Oncol.* 2005;77:18–24.
5. Höckel M, Vormdran B, Schlenger K, Baussmann E, Knapstein PG. Tumor oxygenation: a new predictive parameter in locally advanced cancer of the uterine cervix. *Gynecol Oncol.* 1993;51:141–149.
6. Nordmark M, Lancaster J, Chou SC, et al. Invasive oxygen measurements and pimonidazole labeling in human cervix carcinoma. *Int J Radiat Oncol Biol Phys.* 2001;49:581–586.
7. Nordmark M, Overgaard J. A confirmatory prognostic study on oxygenation status and loco-regional control in advanced head and neck squamous cell carcinoma treated by radiation therapy. *Radiother Oncol.* 2000;57:39–43.
8. Gaertner FC, Souvatzoglou M, Brix G, Beer AJ. Imaging of hypoxia using PET and MRI. *Curr Pharm Biotechnol.* 2012;13:552–570.
9. Bobko AA, Dhimitruka I, Eubank TD, Marsh CB, Zweier JL, Khramtsov VV. Trityl-based EPR probe with enhanced sensitivity to oxygen. *Free Radic Biol Med.* 2009;47:654–658.
10. Yasui H, Matsumoto S, Devasahayam N, et al. Low-field magnetic resonance imaging to visualize chronic and cycling hypoxia in tumor-bearing mice. *Cancer Res.* 2010;70:6427–6436.
11. Dehdashti F, Mintun MA, Lewis JS, et al. In vivo assessment of tumor hypoxia in lung cancer with  $^{60}Cu$ -ATSM. *Eur J Nucl Med Mol Imaging.* 2003;30:844–850.
12. Dehdashti F, Grigsby PW, Lewis JS, Laforest R, Siegel BA, Welch MJ. Assessing tumor hypoxia in cervical cancer by PET with  $^{60}Cu$ -labeled diacetyl-bis(N4-methylthiosemicarbazone). *J Nucl Med.* 2008;49:201–205.
13. Dietz DW, Dehdashti F, Grigsby PW, et al. Tumor hypoxia detected by positron emission tomography with  $^{60}Cu$ -ATSM as a predictor of response and survival in patients undergoing neoadjuvant chemoradiotherapy for rectal carcinoma: a pilot study. *Dis Colon Rectum.* 2008;51:1641–1648.
14. Carlin S, Zhang H, Reese M, Ramos NN, Chen Q, Ricketts SA. A comparison of the imaging characteristics and microregional distribution of 4 hypoxia PET tracers. *J Nucl Med.* 2014;55:515–521.
15. Dence CS, Ponde DE, Welch MJ, Lewis JS. Autoradiographic and small-animal PET comparisons between  $^{18}F$ -FMISO,  $^{18}F$ -FDG,  $^{18}F$ -FLT and the hypoxic selective  $^{64}Cu$ -ATSM in a rodent model of cancer. *Nucl Med Biol.* 2008;35:713–720.
16. Hueting R, Kersemans V, Cornelissen B, et al. A comparison of the behavior of  $^{64}Cu$ -acetate and  $^{64}Cu$ -ATSM in vitro and in vivo. *J Nucl Med.* 2014; 55:128–134.
17. Kersemans V, Cornelissen B, Hueting R, et al. Hypoxia imaging using PET and SPECT: the effects of anesthetic and carrier gas on [Cu]-ATSM, [Tc]-HL91 and [F]-FMISO tumor hypoxia accumulation. *PLoS One.* 2011;6:e25911.
18. Lewis JS, Sharp TL, Laforest R, Fujibayashi Y, Welch MJ. Tumor uptake of copper-diacetyl-bis(N4-methylthiosemicarbazone): effect of changes in tissue oxygenation. *J Nucl Med.* 2001;42:655–661.
19. Matsumoto K, Szajek L, Krishna MC, et al. The influence of tumor oxygenation on hypoxia imaging in murine squamous cell carcinoma using [ $^{64}Cu$ ]Cu-ATSM or [ $^{18}F$ ]fluoromisonidazole positron emission tomography. *Int J Oncol.* 2007; 30:873–881.
20. McCall KC, Humm JL, Bartlett R, Reese M, Carlin S. Copper-64-diacetyl-bis(N4-methylthiosemicarbazone) pharmacokinetics in FaDu xenograft tumors and correlation with microscopic markers of hypoxia. *Int J Radiat Oncol Biol Phys.* 2012;84:e393–e399.
21. O'Donoghue JA, Zanzonico P, Pugachev A, et al. Assessment of regional tumor hypoxia using  $^{18}F$ -fluoromisonidazole and  $^{64}Cu$ (II)-diacetyl-bis(N4-methylthiosemicarbazone) positron emission tomography: comparative study featuring microPET imaging,  $Po_2$  probe measurement, autoradiography, and fluorescent microscopy in the R3327-AT and FaDu rat tumor models. *Int J Radiat Oncol Biol Phys.* 2005; 61:1493–1502.

22. Oh M, Tanaka T, Kobayashi M, et al. Radio-copper-labeled Cu-ATSM: an indicator of quiescent but clonogenic cells under mild hypoxia in a Lewis lung carcinoma model. *Nucl Med Biol.* 2009;36:419–426.
23. Tanaka T, Furukawa T, Fujieda S, Kasamatsu S, Yonekura Y, Fujibayashi Y. Double-tracer autoradiography with Cu-ATSM/FDG and immunohistochemical interpretation in four different mouse implanted tumor models. *Nucl Med Biol.* 2006;33:743–750.
24. Valtorta S, Belloli S, Sanvito F, et al. Comparison of <sup>18</sup>F-fluoroazomycin-arabinofuranoside and <sup>64</sup>Cu-diacetyl-bis(N4-methylthiosemicarbazone) in preclinical models of cancer. *J Nucl Med.* 2013;54:1106–1112.
25. Yuan H, Schroeder T, Bowsher JE, Hedlund LW, Wong T, Dewhirst MW. Intertumoral differences in hypoxia selectivity of the PET imaging agent <sup>64</sup>Cu(II)-diacetyl-bis(N4-methylthiosemicarbazone). *J Nucl Med.* 2006;47:989–998.
26. Hansen AE, Kristensen AT, Law I, McEvoy FJ, Kjaer A, Engelholm SA. Multimodality functional imaging of spontaneous canine tumors using <sup>64</sup>Cu-ATSM and <sup>18</sup>FDG PET/CT and dynamic contrast enhanced perfusion CT. *Radiother Oncol.* 2012;102:424–428.
27. Maurer RI, Blower PJ, Dilworth JR, Reynolds CA, Zheng Y, Mullen GE. Studies on the mechanism of hypoxic selectivity in copper bis(thiosemicarbazone) radiopharmaceuticals. *J Med Chem.* 2002;45:1420–1431.
28. Obata A, Yoshimi E, Waki A, et al. Retention mechanism of hypoxia selective nuclear imaging/radiotherapeutic agent cu-diacetyl-bis(N4-methylthiosemicarbazone) (Cu-ATSM) in tumor cells. *Ann Nucl Med.* 2001;15:499–504.
29. Donnelly PS, Liddell JR, Lim S, et al. An impaired mitochondrial electron transport chain increases retention of the hypoxia imaging agent diacetyl-bis(4-methylthiosemicarbazone)copperII. *Proc Natl Acad Sci USA.* 2012;109:47–52.
30. Burgman P, O'Donoghue JA, Lewis JS, Welch MJ, Humm JL, Ling CC. Cell line-dependent differences in uptake and retention of the hypoxia-selective nuclear imaging agent Cu-ATSM. *Nucl Med Biol.* 2005;32:623–630.
31. Liu J, Hajibeigi A, Ren G, et al. Retention of the radiotracers <sup>64</sup>Cu-ATSM and <sup>64</sup>Cu-PTSM in human and murine tumors is influenced by MDR1 protein expression. *J Nucl Med.* 2009;50:1332–1339.
32. Price KA, Crouch PJ, Volitakis I, et al. Mechanisms controlling the cellular accumulation of copper bis(thiosemicarbazone) complexes. *Inorg Chem.* 2011;50:9594–9605.
33. Jørgensen JT, Persson M, Madsen J, Kjaer A. High tumor uptake of <sup>64</sup>Cu: implications for molecular imaging of tumor characteristics with copper-based PET tracers. *Nucl Med Biol.* 2013;40:345–350.
34. Peng F, Lu X, Janisse J, Muzik O, Shields AF. PET of human prostate cancer xenografts in mice with increased uptake of <sup>64</sup>CuCl<sub>2</sub>. *J Nucl Med.* 2006;47:1649–1652.
35. Busk M, Horsman MR, Jakobsen S, et al. Imaging hypoxia in xenografted and murine tumors with <sup>18</sup>F-fluoroazomycin arabinoside: a comparative study involving microPET, autoradiography, PO<sub>2</sub>-polarography, and fluorescence microscopy. *Int J Radiat Oncol Biol Phys.* 2008;70:1202–1212.
36. Gagel B, Piroth M, Pinkawa M, et al. pO polarography, contrast enhanced color duplex sonography (CDS), [<sup>18</sup>F] fluoromisonidazole and [<sup>18</sup>F] fluorodeoxyglucose positron emission tomography: validated methods for the evaluation of therapy-relevant tumor oxygenation or only bricks in the puzzle of tumor hypoxia? *BMC Cancer.* 2007;7:113.
37. Tran LB, Bol A, Labar D, et al. Hypoxia imaging with the nitroimidazole <sup>18</sup>F-FAZA PET tracer: a comparison with OxyLite, EPR oximetry and <sup>19</sup>F-MRI relaxometry. *Radiother Oncol.* 2012;105:29–35.
38. Bartlett RM, Beattie BJ, Naryanan M, et al. Image-guided PO<sub>2</sub> probe measurements correlated with parametric images derived from <sup>18</sup>F-fluoromisonidazole small-animal pet data in rats. *J Nucl Med.* 2012;53:1608–1615.
39. Chang J, Wen B, Kazanzides P, et al. A robotic system for <sup>18</sup>F-FMISO PET-guided intratumoral pO<sub>2</sub> measurements. *Med Phys.* 2009;36:5301–5309.